P1.1 **Comparison of Turbulence Closure Schemes in the Simulation of Terrain-disrupted Airflow**

P.W. Chan *
Hong Kong Observatory, Hong Kong, China

1. INTRODUCTION

Hong Kong International Airport (HKIA) is situated in an area of complex terrain. To the south of the airport is the mountainous Lantau Island with peaks rising to about 1000 m AMSL and valleys as low as 400 m in between. Turbulent airlfow due to terrain disruption could occur at the airport area when the winds from east to southwest climb over Lantau Island. The Hong Kong Observatory (HKO) provides turbulence alerting services to HKIA. In accordance with the practice of the International Civil Aviation Organization (ICAO), turbulence intensity is expressed in terms of the cube root of the turbulent kinetic energy (TKE) dissipation rate, or eddy dissipation rate (EDR). An $EDR^{1/3}$ between 0.3 and 0.5 $m^{2/3}s^{-1}$ refers to moderate turbulence, and $EDR^{1/3}$ of 0.5 $m^{2/3}s^{-1}$ or above is severe turbulence.

High-resolution numerical simulation provides useful insight into the nature of turbulent airflow in the vicinity of HKIA. Chan (2006a) studied the terrain-induced turbulence using the Regional Atmospheric Modelling System (RAMS) version 4.4 with a horizontal resolution of 50 m. The Deardorff (1980) turbulence parameterization scheme was adopted, with the dissipation term in the TKE equation directly used for comparison with EDR observations from a LIght Detection And Ranging (LIDAR) system and a wind profiler in two selected cases. The model simulated EDR field was found to capture the salient features of the horizontal variation of turbulence intensity in these cases of terrain-disrupted airlfow. However, in general the EDR drops with height too rapidly in comparison with the real data.

The choice of turbulence parameterization scheme in the numerical model affects the simulation result of EDR distribution. Besides the schemes of Mellor and Yamada (1982) level 2.5 closure and Deardorff (1980), the latest version of RAMS (i.e. version 6.0) also includes newly developed schemes such as *e-l* scheme of Trini Castelli et al. (2005). In this paper, the performance of these three turbulence parameterization schemes was studied in an idealized simulation of the airflow over a three-dimensional isolated hill. The present work is the first study to compare these three schemes in real cases. The TKE schemes are briefly reviewed in Section 2. The model setup is discussed in Section 3. Simulation results are presented in Section 4 and conclusions are drawn in Section 5.

2. TKE SCHEMES

A summary of the TKE schemes available in RAMS could be found in Trini Castelli et al. (2005). Only a summary is given here. In Mellor and Yamada (1982) scheme, the TKE dissipation rate ε is determined from the following equation:

$$\varepsilon = \frac{(2e)^{3/2}}{\Lambda} \qquad (1)$$

where e is the TKE and Λ is proportional to the mixing length l. The Blackadar (1962) formulation of l is employed:

$$l = \frac{kz}{1 + kz/l_\infty} \qquad (2)$$

where k is the von Karman constant (0.4) and l_∞ is an asymptotic value defined by:

$$l_\infty = a_\infty \frac{\int z\sqrt{e}dz}{\int \sqrt{e}dz} \qquad (3)$$

where a_∞ is taken to be 0.1.

In Deardorff (1980) scheme, ε is given by:

$$\varepsilon = \frac{C_D e^{3/2}}{l} \qquad (4)$$

where l is taken to be Δx (the grid size in x direction) in neutral case and $C_D = 0.19 + (0.51l) / (\Delta x\, \Delta y\, \Delta z)^{1/3}$.

Analogous to the Deardorff (1980) scheme, the *e-l* scheme is also based on a complete TKE equation, together with an analytical parameterization of the mixing length. The dissipation term is similar to Equation (4), but with a different empirical constant C_ε in place of C_D. Details of the estimation of this empirical constant could be found in Trini Castelli et al. (2005). Moreover, mixing length l is determined from the Blackadar (1962) formulation (Equation (2)), but with l_∞ given by $0.009u_*/f$, where u_* and f are the friction velocity and Coriolis parameter respectively.

3. MODEL SETUP

The RAMS model is nested with the operational Regional Spectral Model of HKO, which has a horizontal resolution of 20 km. The model domains are similar to those in Chan (2006a). Four nesting runs are performed with RAMS, with horizontal resolution of 4 km, 800 m, 200 m and 50 m. The innermost domain just focuses on the area to the west of HKIA, which is downwind of the mountains on Lantau Island in easterly to southwesterly flow.

Mellor and Yamada (1982) level 2.5 scheme is applied to grids 1, 2 and 3. The three different turbulence parameterization schemes described in

* *Corresponding author address:* P.W. Chan, Hong Kong Observatory, 134A Nathan Road, Hong Kong email: pwchan@hko.gov.hk

Section 2 are separately applied in gird 4 (i.e. the innermost domain) and the simulation results are compared in the next Section.

4. COMPARISON OF SIMULATION RESULTS

Two cases are studied in this paper. The first case has been considered in Chan (2006a), viz. a spring-time easterly wind case. On 1 and 2 February 2006, a strong east to southeasterly airstream prevailed in the vicinity of HKIA. This paper focuses at the time when reversed flow occurred to the southwest of the airport (Figure 1), i.e. about 19 UTC, 1 February 2006 (=3 a.m., 2 February HKT, with HKT = UTC + 8 hours). The area of reversed flow appeared to be associated with the wake of the tall mountains on Lantau Island.

An EDR map (Figure 2) at the same time is calculated from the LIDAR's radial velocity data using the longitudinal structure function approach (Chan, 2006b). It shows that EDR is mostly in the region of 0.25 $m^{2/3}s^{-1}$ over the airport and the sea to the west, including the area of reversed flow. There are also tiny streaks (with a width of several hundred metres) of more turbulent airflow (with EDR in the order of 0.35 to 0.5 $m^{2/3}s^{-1}$) emanating from the northern part of Nei Lak Shan (location in Figure 1). On the other hand, the sea area to the north of HKIA appears to have more uniform flow and the EDR is much lower (about 0.1 to 0.15 $m^{2/3}s^{-1}$ only).

The simulated EDR fields using the Mellor-Yamada, Deardorff and *e-l* scheme are given in Figures 3 to 5 respectively. The simulation is initialized at 18 UTC, 1 February 2006. All the three schemes are able to forecast the airlfow with moderate turbulence to the southwest of HKIA. Overall speaking, Deardorff scheme appears to perform the best because it reproduces the moderate turbulence over the airport and the streaks of more turbulent airflow downstream of Nei Lak Shan. Mellor-Yamada scheme gives too weak turbulence over the airport. The *e-l* scheme seems to create too much mixing (as could be seen from the rather "wavy" streamline at 50 m AMSL in the reversed flow area to the southwest of HKIA) and lead to too weak turbulence over the sea directly to the west of the airport (with EDR in the order of 0.1 $m^{2/3}s^{-1}$ only).

The forecast EDR profile at the location of the Sha Lo Wan wind profiler (location in Figure 1) is also compared with the observed profile (Figure 6). In general, the profile given by Deardorff scheme has the right magnitude as compared to the actual observations, though it fluctuates rather rapidly with height. The profile given by Mellor-Yamada scheme shows similar variation with altitude as the actual profile, but the magnitude is generally smaller. The *e-l* scheme creates significant mixing near the ground, but then the EDR drops rapidly with height in the first couple of hundred metres above ground and maintains at relatively low values aloft.

To examine the performance of the model forecasts in another wind regime, a strong southwest monsoon case in the summer, viz. 8 June 2006 (about 23 UTC, 7 June 2006) is considered. The LIDAR's radial velocity data are shown in Figure 7, and the corresponding LIDAR EDR map is give in Figure 8. It is observed that the moderate turbulence (EDR of 0.25 – 0.3 $m^{2/3}s^{-1}$) appears over HKIA and southwest of the airport. In this region, there are also tiny blobs of more turbulent flow (EDR of 0.35 to 0.5 $m^{2/3}s^{-1}$) embedded inside, each with a spatial scale of several hundred metres. Over the sea area much further west and north of the airport (beyond 1-2 nautical miles or so), the airflow is less turbulent (EDR of 0.1 $m^{2/3}s^{-1}$) possibly due to insignificant terrain disruption.

The forecast EDR maps with the three turbulence parameterization schemes are shown in Figures 9 to 11. The Mellor-Yamada and Deardorff schemes reproduce the main features of the observed EDR maps fairly well. However, the former appears to underestimate and the latter overestimate the turbulence intensity associated with the blobs of more turbulent flow directly over and to the southwest of HKIA. The *e-l* scheme does not give the observed moderate turbulence area to the southwest of the airport.

Unfortunately, Sha Lo Wan wind profiler observations are not available in this southwest monsoon case. To study the vertical profile of turbulence intensity, the LIDAR's vertical cross-section data at 258 degrees azimuth are used. EDR is determined in a way similar to the conical scans (Chan, 2006b), again using longitudinal structure function approach. The EDR profile at a location of about 2 km to the west-southwest of the LIDAR is considered (Figure 7). The measured profile and the simulation results are compared in Figure 12. Below 300 m AMSL or so, the measured profile and the results of Mellor-Yamada and Deardorff schemes have similar magnitude. Between 300 and 800 m, the forecast profiles drop too rapidly in comparison to the measured profile. For the altitudes aloft, Deardorff appears to capture the peak of EDR near the top of the boundary layer (about 1300 m AMSL). As in the spring-time easterly wind case, the *e-l* scheme gives too large EDR near the ground, and the turbulence intensity drops with height too rapidly so that it shows the largest deviation from the measurement results.

5. CONCLUSIONS

The choice of turbulence parameterization scheme has profound impact on the forecast turbulence intensity distribution in terrain-disrupted airlfow in the vicinity of HKIA. Three schemes available in the latest version of RAMS (viz. version 6.0) are considered, namely, the Mellor-Yamada scheme and Deardorff scheme, as well as the new *e-l* scheme. The forecast results are compared with the actual observations of EDR from LIDAR and wind profiler in two distinct wind regimes, i.e. east to southeasterly wind case in the spring and southwest monsoon in the summer.

In the two cases, Deardorff scheme is found to perform the best in reproducing the spatial variation of EDR in comparison to the actual observations. However, it appears to over-predict the turbulence intensity and the areal extent of severe turbulent flow just downstream of the mountains of Lantau Island.

The vertical EDR profile, though in general having similar magnitudes as the actual observations, could either show too many fluctuations or drop too rapidly with altitude in the middle part of the boundary layer. Mellor-Yamada scheme also gives a reasonable distribution of EDR in the vicinity of HKIA, but it tends to underestimate the turbulence intensity downstream of the mountains of Lantau Island and the EDR values are generally smaller than the actual measurements in the vertical profiles. The *e-l* scheme appears to create too much mixing near the ground, so that the near-ground EDR value could be unrealistically large compared to the actual measurement. On the other hand, the EDR delays too rapidly with the horizontal distance away from the terrain as well as with the altitude.

It is expected that the results in this paper would serve as a useful reference for modellers in choosing the appropriate turbulence parameterization schemes in forecasting turbulence intensity in terrain-disrupted airlfow and further developing the schemes to better reproduce the actual observations.

References

Blackadar, A.K., 1962: The vertical distribution of wind and turbulent exchange in a neutral Atmosphere, *J. Geophys. Res.*, **67**, 3095–3102.

Chan, P.W., 2006a: Super-high-resolution numerical simulation of atmospheric turbulence in an area of complex terrain. *12th Conference on Mountain Meteorology*, American Meteorological Society.

Chan, P.W., 2006b: Generation of eddy dissipation rate map at the Hong Kong International Airport based on Doppler LIDAR data. *12th Conference on Aviation, Range, and Aerospace Meteorology*, American Meteorological Society.

Deardorff, J.W., 1980: Stratocumulus-capped mixed layers derived from a three-dimensional model. *Bound.-Layer Meteor.*, **18**, 495–527.

Mellor, G. L., and T. Yamada, 1982: Development of a turbulence closure model for geophysical fluid problems. *Rev. Geophys. Space Phys.*, **20**, 851–875.

Trini Castelli, S., E. Ferrero, D. Anfossi, and R. Ohba, 2005: Turbulence closure models and their application in RAMS. *Environmental Fluid Mechanics,* **5**, 169–192.

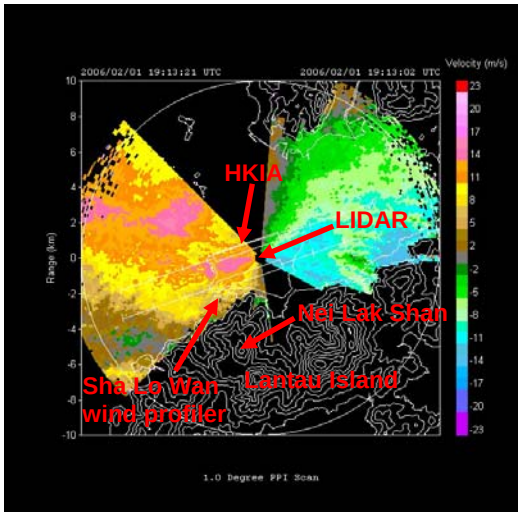

Figure 1 LIDAR's radial velocity at 1-degree elevation conical scan at 19:13 UTC, 1 February 2006.

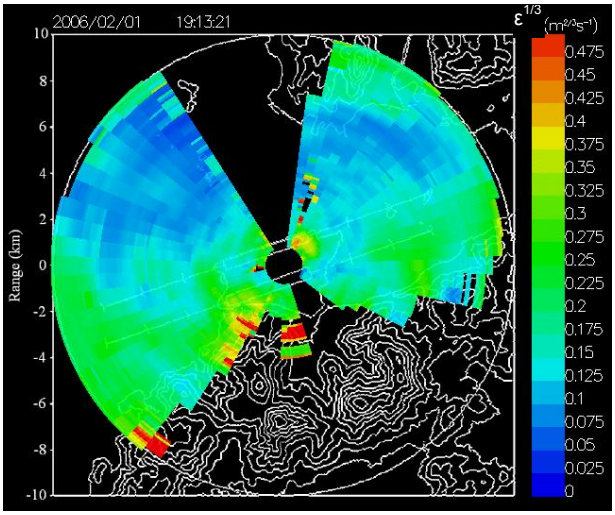

Figure 2 EDR map based on LIDAR data at the same time as Figure 1.

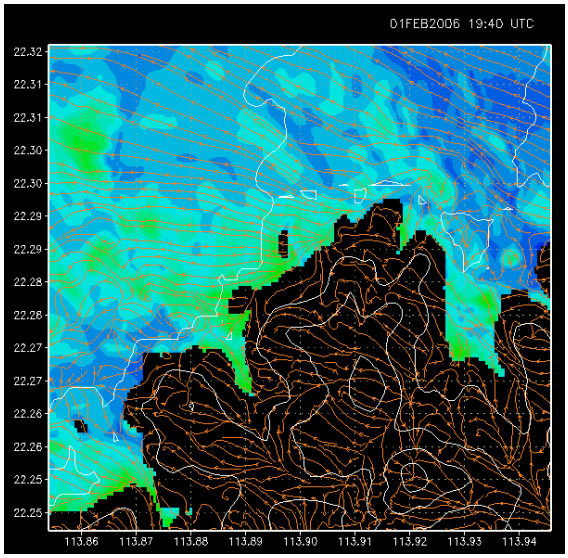

Figure 3 Forecast EDR field at 50 m AMSL at the same time of Figure 2 using Mellor-Yamada scheme. The scale of EDR is the same as Figure 2.

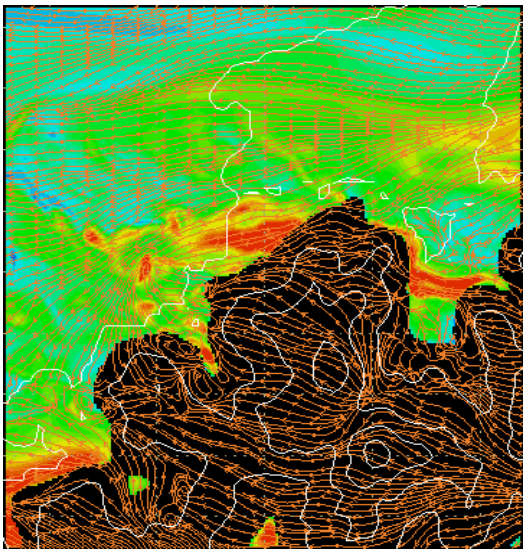

Figure 4 Forecast EDR field at 50 m AMSL at the same time of Figure 2 using Deardorff scheme. The scale of EDR is the same as Figure 2.

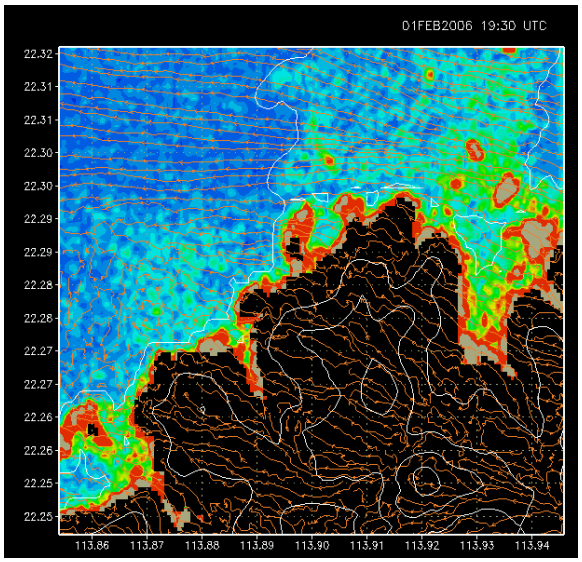

Figure 5 Forecast EDR field at 50 m AMSL at the same time of Figure 2 using *e-l* scheme. The scale of EDR is the same as Figure 2. Grey means $\varepsilon^{1/3} > 0.5$.

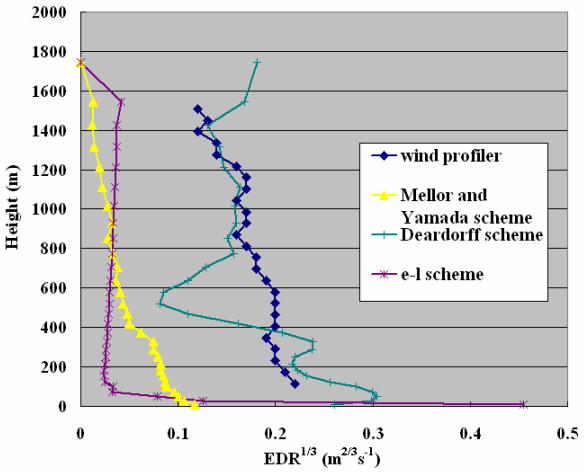

Figure 6 The observed and the forecast EDR profiles at Sha Lo Wan at the same time as Figure 2. The forecast profiles are hourly averages to remove short-term fluctuations.

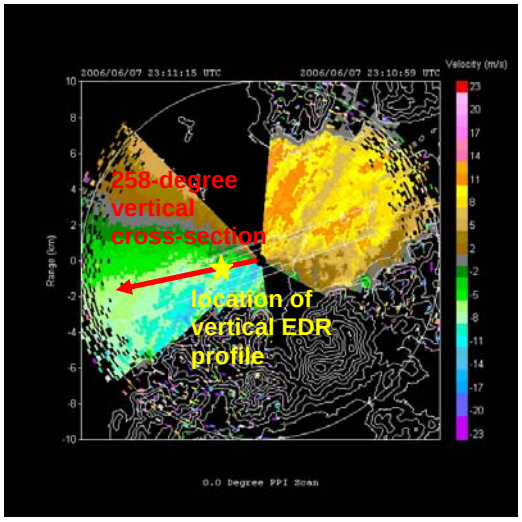

Figure 7 LIDAR's radial velocity at horizontal scan at 23:11 UTC, 7 June 2006.

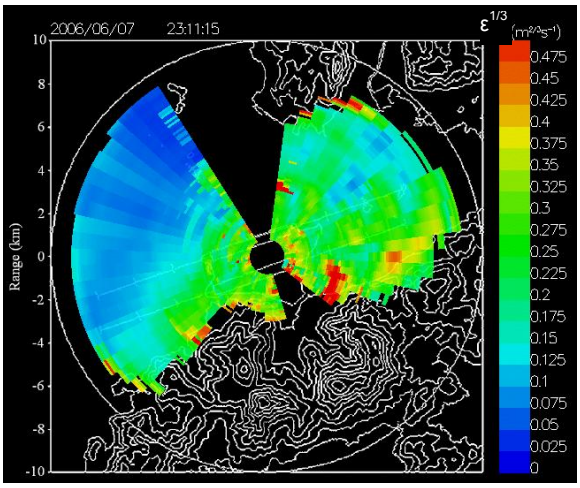

Figure 8 EDR map based on LIDAR's radial velocity data at the same time as Figure 7.

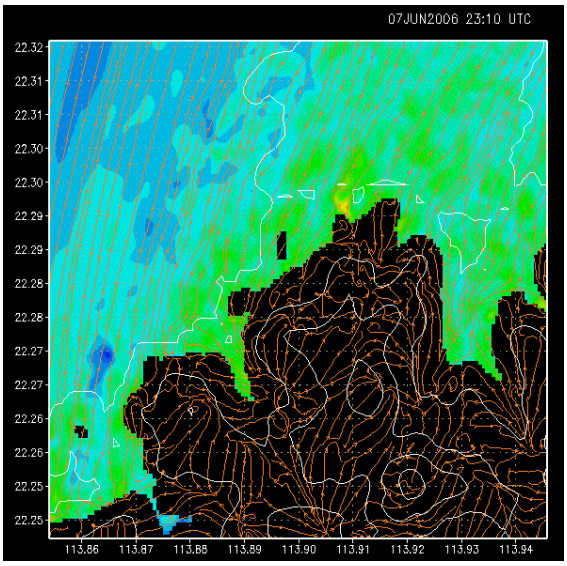

Figure 9 Forecast EDR field at 50 m AMSL at the same time of Figure 8 using Mellor-Yamada scheme. The scale of EDR is the same as Figure 8.

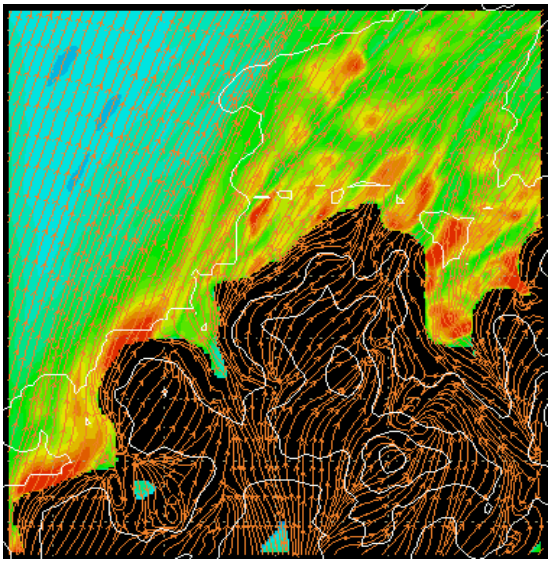

Figure 10 Forecast EDR field at 50 m AMSL at the same time of Figure 8 using Deardorff scheme. The scale of EDR is the same as Figure 8.

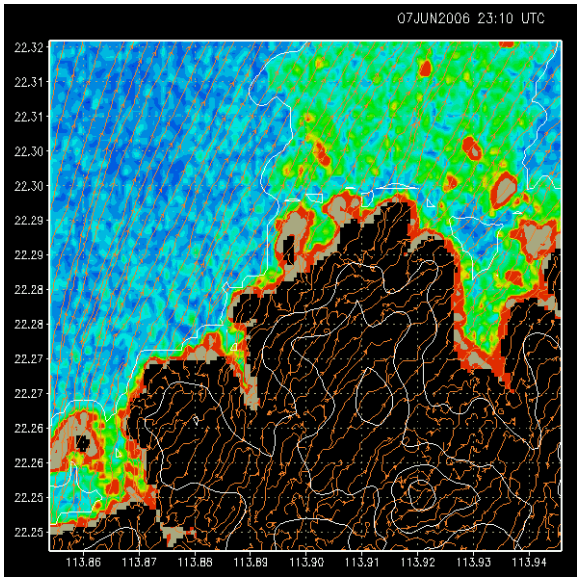

Figure 11 Forecast EDR field at 50 m AMSL at the same time of Figure 8 using *e-l* scheme. The scale of EDR is the same as Figure 8. Grey means $\varepsilon^{1/3} > 0.5$.

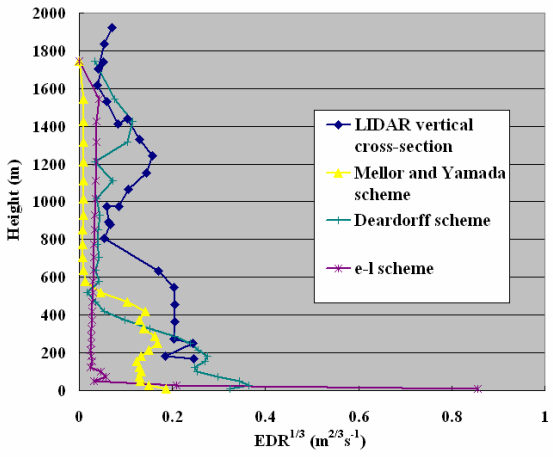

Figure 12 The observed and the forecast EDR profiles at the location indicated in Figure 7 at the same time as Figure 8. The forecast profiles are hourly averages to remove short-term fluctuations.